JOURNAL OF MATERIALS SCIENCE 31 (1996) 31–37

Low temperature iron thin film–silicon reactions

N. R. BALDWIN, D. G. IVEY
Department of Mining, Metallurgical and Petroleum Engineering, University of Alberta, Edmonton, Alberta, Canada T6G 2G6

Low temperature reactions between Fe thin films and Si substrates have been studied. Iron films were deposited by electron beam evaporation onto ⟨1 1 1⟩ orientated Si substrates. An SiO_2 capping layer was used to protect the Fe from oxidation during subsequent annealing. Samples were annealed at temperatures as high as 650 °C, for up to several hours. It has been shown that FeSi is the initial silicide to form, with 300 °C being the lowest formation temperature. Fe_3Si forms after most of the Fe has been consumed, and forms as a separate phase from α-Fe and not through a disorder–order transformation. Microstructural evidence for nucleation controlled formation of β-$FeSi_2$ from FeSi has also been given.

1. Introduction

There has been considerable interest in iron silicides recently, and in particular semiconducting β-$FeSi_2$. The band gap of β-$FeSi_2$, which has been measured by several groups [1–14], with a value of 0.8–0.9 eV reported in most cases, is potentially suitable for optoelectronic applications. It remains to be seen whether high quality thin films of β-$FeSi_2$ can be grown on Si, thereby making $FeSi_2$ compatible with existing silicon based integrated circuit technology.

A number of thin film studies have been done on the Fe–Si system. In most cases the lower temperature reactions have been ignored in favour of higher temperature ones, with the aim of forming β-$FeSi_2$. Other silicides that are thermodynamically stable at low temperatures ($\leqslant 800$ °C) include FeSi and Fe_3Si, the latter has two structural variations, α_1 and α_2. The work that has been done on deposited Fe films on Si substrates, which are subsequently annealed, is briefly outlined below.

The most Fe-rich silicide is Fe_3Si, which according to the Fe–Si phase diagram (Fig. 1) has a wide range of stoichiometry. Both forms of Fe_3Si are cubic; the α_1 form has a lattice parameter of 0.5640 nm, while $a = 0.2840$ nm for the α_2 form. Fe_3Si has been reported to form during low temperature annealing of Fe thin film–Si couples [15–17]. In the study done by Lau *et al.* [17], α_1-Fe_3Si is reported to be the initial silicide to form through a disorder–order transition.

The monosilicide, stoichiometric FeSi, is reported to be the initial silicide to form in most low temperature studies [3, 15, 16, 19–22]. It has a cubic structure with $a = 0.449$ nm and has been reported to form at temperatures as low as 200 °C, for thin layers of Fe (2 nm) deposited under ultra high vacuum (UHV) conditions. For thicker layers (> 10 nm) and conventional vacuum levels, the lowest reported formation temperature is 400 °C. At higher annealing temperatures (> 450 °C), β-$FeSi_2$ forms at the expense of FeSi. This silicide remains stable to ≈ 940 °C, whereupon it progressively transforms into the metallic α-$FeSi_2$ form, which has an even higher atomic percentage of Si than β-$FeSi_2$ because $\approx 13\%$ of its Fe sites are vacant. β-$FeSi_2$ is orthorhombic with lattice parameters of $a = 0.9863$ nm, $b = 0.7791$ nm and $c = 0.7833$ nm, while α-$FeSi_2$ is tetragonal with $a = 0.264$ nm and $b = 0.783$ nm.

Recently, two metastable silicides, γ-$FeSi_2$ and $FeSi_{(CsCl)}$, have been reported in the literature [23–30]. γ-$FeSi_2$ is cubic with $a = 0.5389$ nm, which is very close to the lattice parameter of Si. $FeSi_{(CsCl)}$ is also cubic, with a CsCl type structure. Both phases grow pseudomorphically on Si substrates, only when the ratio of interfacial area (with Si) to silicide volume is very large, i.e. for thin Fe layers of the order of a few nanometres or less.

Very little has been done on the growth kinetics of iron silicides. One of the few studies was done in 1975 by Lau *et al.* [17], using Rutherford backscattering spectrometry (RBS) to measure the thickness of FeSi formed as 100–150 nm thick Fe films on single crystal Si were annealed. FeSi growth was found to be diffusion controlled, with Si being the dominant diffuser, and an activation energy for FeSi growth was calculated from the kinetic data to be 1.67 ± 0.15 eV or 161 ± 14 kJ mol^{-1}. Formation rates of FeSi seemed to be slightly higher on the Si (1 1 1) substrates than on the Si (1 0 0) substrates. More recently, Radermacher *et al.* performed similar experiments to determine the growth kinetics of iron silicide films [31]. The main procedural difference between the two investigations is that Radermacher *et al.* used rapid thermal annealing instead of conventional annealing. The activation energy for FeSi diffusion controlled growth on Si (1 1 1) was determined to be 1.36 ± 0.25 eV or 131 ± 24 kJ mol^{-1}, somewhat lower than the result in [17]. The choice of annealing procedure was given as a possible factor in this difference.

The formation of β-$FeSi_2$ is generally considered to be nucleation controlled [7, 31, 32]. In a study done

0022–2461 © 1996 Chapman & Hall

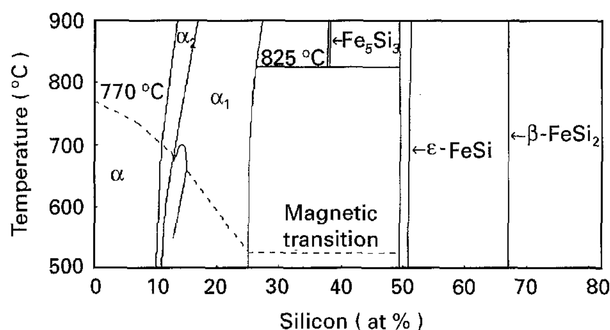

Figure 1 Lower temperature, Fe-rich region of the Fe–Si phase diagram [18].

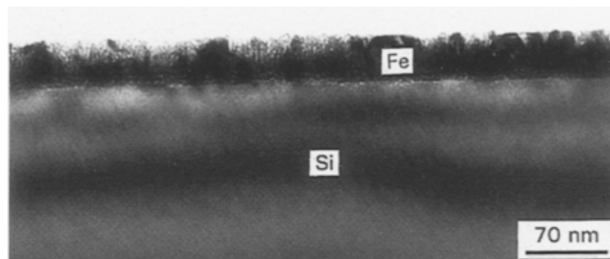

Figure 2 TEM cross-section image from an as-deposited sample.

by Erlesand *et al.* [32], the activation energy for the growth of β-$FeSi_2$ on amorphous Si was calculated to be 1.5 ± 0.1 eV or 150 kJ $\pm$ 10 kJ mol^{-1}. In marker experiments, carried out to determine the major diffusing species during the formation of β-$FeSi_2$ from FeSi, marker displacement was small but appeared to demonstrate that Si was the major diffuser. Dimitriadis and Werner [7] have proposed that β-$FeSi_2$ forms by an "explosive crystallization" process. The heat released during the formation of β-$FeSi_2$ from FeSi travels outward from a nucleation site as a circular heat wave, which is not quickly conducted away because of the low thermal conductivities of the materials involved.

Radermacher *et al.* [31] has also determined the activation energy for β-$FeSi_2$ formation, although thickness measurements were taken from relatively thick disilicide films that had passed the nucleation controlled stage and moved on to diffusion controlled kinetics. The activation energy for the diffusion controlled growth of β-$FeSi_2$ films on Si (1 1 1) was calculated to be 2.6 ± 0.5 eV or 250 ± 50 kJ mol^{-1}.

The purpose of the present study was to examine low temperature ($\leqslant 650\,°C$) annealing of relatively thick ($\approx$40 nm) Fe films on $\langle 1\,1\,1 \rangle$ orientated Si substrates. The study is focused on initial phase formation (FeSi versus Fe_3Si) and obtaining experimental verification for nucleation controlled formation of β-$FeSi_2$.

2. Experimental procedure

Silicon $\langle 1\,1\,1 \rangle$ orientated wafers doped with boron to a resistivity of 1.0–10.0 $\Omega\,cm^{-1}$ were used. The wafers were cleaned in a 10:1 buffered hydrofluoric acid solution for about 1 min. They were then thoroughly rinsed in deionized water and blown dry with N_2. Immediately after cleaning, the substrates were loaded into the electron beam evaporation chamber and the chamber was evacuated.

Iron films were deposited onto Si (1 1 1) wafers by electron beam evaporation from a 99.95% pure Fe target, which had been degassed. In the same vacuum chamber, a protective capping film of SiO_2 was immediately evaporated on top of the Fe. The capping layer has been found to be necessary to prevent oxidation and agglomeration of the Fe film during *ex situ* annealing. Base pressures were $\sim 5 \times 10^{-6}$ Pa and deposition pressures were $\sim 4 \times 10^{-4}$ Pa for the Fe and $\sim 7 \times 10^{-5}$ Pa for the SiO_2. The Fe was deposited at a rate of $\sim$1.7 nm s^{-1} and the SiO_2 at a rate of $\sim$0.2 nm s^{-1}. Film thicknesses were monitored during deposition by a quartz thickness monitor, but were more accurately determined later by cross-sectional transmission electron microscopy (TEM). The Fe layer was found to be $\sim$40 nm thick; the SiO_2 was $\sim$120 nm thick.

Wafers were cleaved into sections about 1 cm^2 and annealed in a small quartz furnace in a flowing nitrogen atmosphere. Samples were annealed at temperatures ranging from 300 to 650 °C for up to 3 h.

Annealed samples were examined by TEM, using both plan view and cross-section specimens. These were prepared using standard techniques involving a combination of mechanical polishing and ion milling. TEM samples were examined in either a Hitachi H-7000 or a Jeol 2010 equipped with a Ge ultrathin window X-ray detector. Phase analysis was done through a combination of imaging, electron diffraction and X-ray microanalysis.

3. Results and discussion

A TEM cross-section image of the as-deposited sample is shown in Fig. 2. The Fe layer thickness was calculated from micrographs to be about 40 nm, with an average grain size of $\approx$10 nm. This initial Fe layer contains many voids though, because of the low temperature and rapid rate at which it was deposited. By measuring the thickness of completed β-$FeSi_2$ layers (from annealed samples) and knowing the unit cell volume of the disilicide and Fe, the as-deposited layer was found to be equivalent in Fe content to a fully dense layer of about 35 nm.

The lowest annealing temperature studied was 300 °C, with samples annealed for up to 3 h. From cross-section specimens (Fig. 3a), it appears as though no reaction has occurred; the only layer visible is α-Fe. Silicon diffusion has begun, however, as a significant amount of Si is dissolved in the Fe (Fig. 3b). Close examination of a selected area diffraction (SAD) pattern taken from a plan view specimen reveals that there are three additional diffuse rings that cannot be attributed to α-Fe (Fig. 3c); the spots are due to the Si substrate. These rings do not correlate with superlattice lines from either α_1- or α_2-Fe_3Si, but can only be attributed to (1 1 1), (2 1 0) and (2 2 1) planes of FeSi. If α_1-Fe_3Si were present, a reflection at $d = 0.283$ nm should be present, but is missing. For clarity the

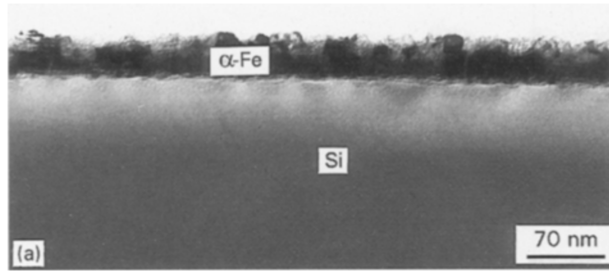

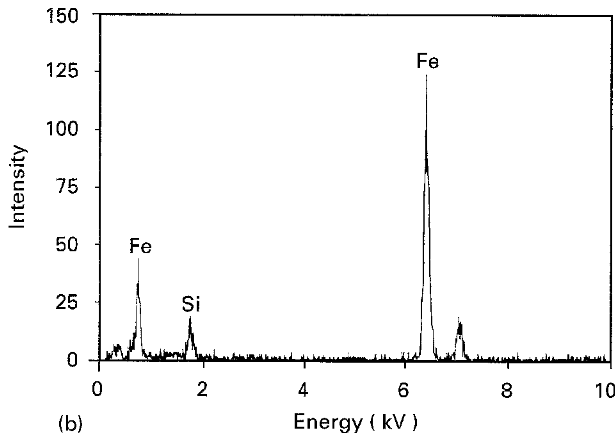

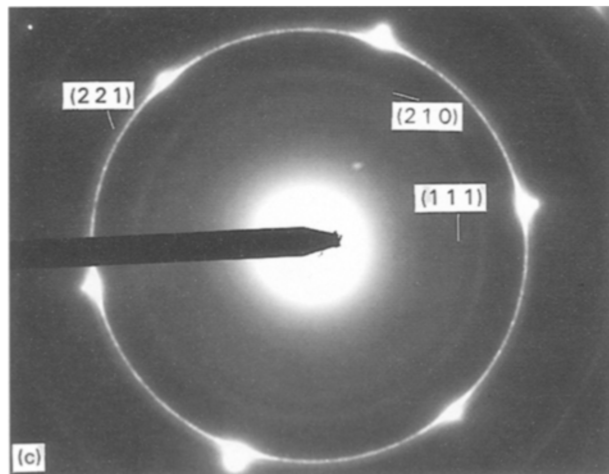

Figure 3 (a) Cross-section image of sample annealed at 300 °C for 2 h, (b) EDX spectrum from the α-Fe layer in Fig. 3a, and (c) SAD pattern taken from a plan view section of the same sample.

diffraction data is tabulated in Table I, which shows that the match with FeSi is quite good. Clearly, FeSi and not Fe_3Si, is the first phase to form at the Fe–Si interface. The volume of material observable in cross-section specimens is extremely small, relative to that in plan view specimens, which would account for the absence of an FeSi layer in the cross-section sample of Fig. 3a.

The silicide formation sequence at 400 °C is illustrated in a series of cross-section micrographs in Fig. 4. SAD patterns from plan view specimens are included with some of the micrographs; the SAD data is also tabulated in Table II, as many of the weak reflections are difficult to see in the SAD patterns. After 30 min of annealing, two distinct layers are visible (Fig. 4a). These were identified primarily through SAD analysis, with verification through energy dispersive X-ray (EDX) analysis. The most intense rings in the SAD pattern of Fig. 4a are from α-Fe (the ≈30 nm thick layer in Fig. 4a), while the faint rings correspond to FeSi (≈10 nm thick inner layer in Fig. 4a). FeSi exhibits preferred orientation with respect to the Si substrate.

$$(1\,1\,1)\,\text{FeSi} \parallel (1\,1\,1)\,\text{Si} \qquad [1\,0\,\bar{1}]\,\text{FeSi} \parallel [2\,\bar{1}\,\bar{1}]\,\text{Si}$$

At least some preferential growth of FeSi on Si was achieved for FeSi thicknesses up to 40–50 nm. For thicker FeSi layers, random orientations were obtained. Preferred growth of FeSi has been reported previously [9, 25, 33–35] for FeSi films thinner than 10 nm.

From the SAD data in Table II, it is clear that Fe_3Si only forms at the longer annealing times (2 h), when most of the α-Fe has been consumed. At shorter annealing times, one could argue that many of the reflections for Fe_3Si and α-Fe have similar *d* spacings (see Table II), which would suggest that Fe_3Si may be present. However, if Fe_3Si were indeed present, additional reflections not common to α-Fe would also be present, e.g. (2 0 0) with $d = 0.2830$ nm. This is not the case. In addition, Fe_3Si is not just an ordered form of the α-Fe solid solution, as small grains of Fe_3Si (identified as α_1) are present between the FeSi layer and the few remaining islands of α-Fe (not visible in Fig. 4c, 2 h anneal at 400 °C). The two phases are microstructurally separate and distinctly different in composition, as demonstrated in the EDX spectra taken from α-Fe, Fe_3Si and FeSi (Fig. 5). The number of counts in the EDX spectra is not high, due to the thin nature of the layers, so only qualitative comparisons can be made. However, it is quite evident that Si levels in Fe_3Si are significantly higher than in α-Fe. The Si concentration is approximately constant in Fe_3Si as well, suggesting that Fe_3Si is stoichiometric. These

TABLE I Indexed SAD results for 300 °C sample

d (nm)	Intensity	Si *d* (nm)	Si *h k l*	α-Fe *d* (nm)	α-Fe *h k l*	FeSi *d* (nm)	FeSi *h k l*
0.2529	Weak, prefer					0.2591	(1 1 1)
0.2035	Strongest			0.2027	(1 1 0)		
0.1978	Weak					0.2008	(2 1 0)
0.1920	Spots	0.1920	(2 2 0)				
0.1485	Weak					0.1496	(2 2 1)
0.1433	Strong			0.1433	(2 0 0)	0.1419	(3 1 0)
0.1177	Strong			0.1170	(2 1 1)	0.1199	(3 2 1)

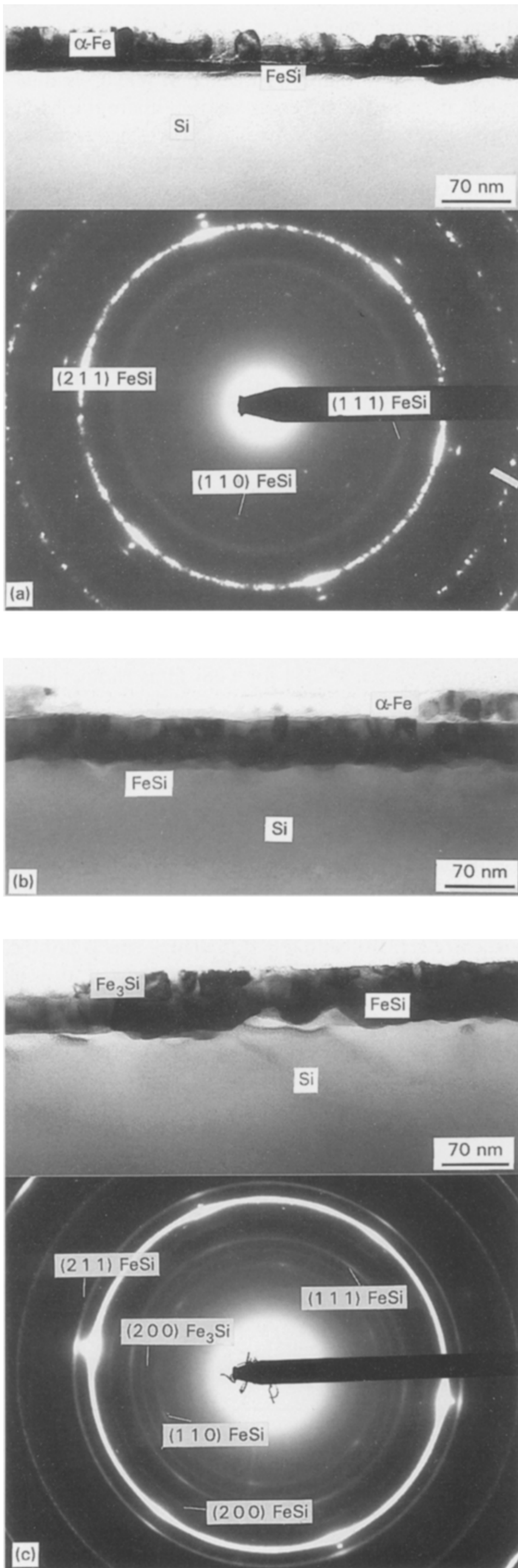

Figure 4 Cross-section images and SAD patterns of samples annealed at 400 °C: (a) 30 min, (b) 60 min, and (c) 2 h. The FeSi and Fe_3Si reflections in the SAD patterns are labelled.

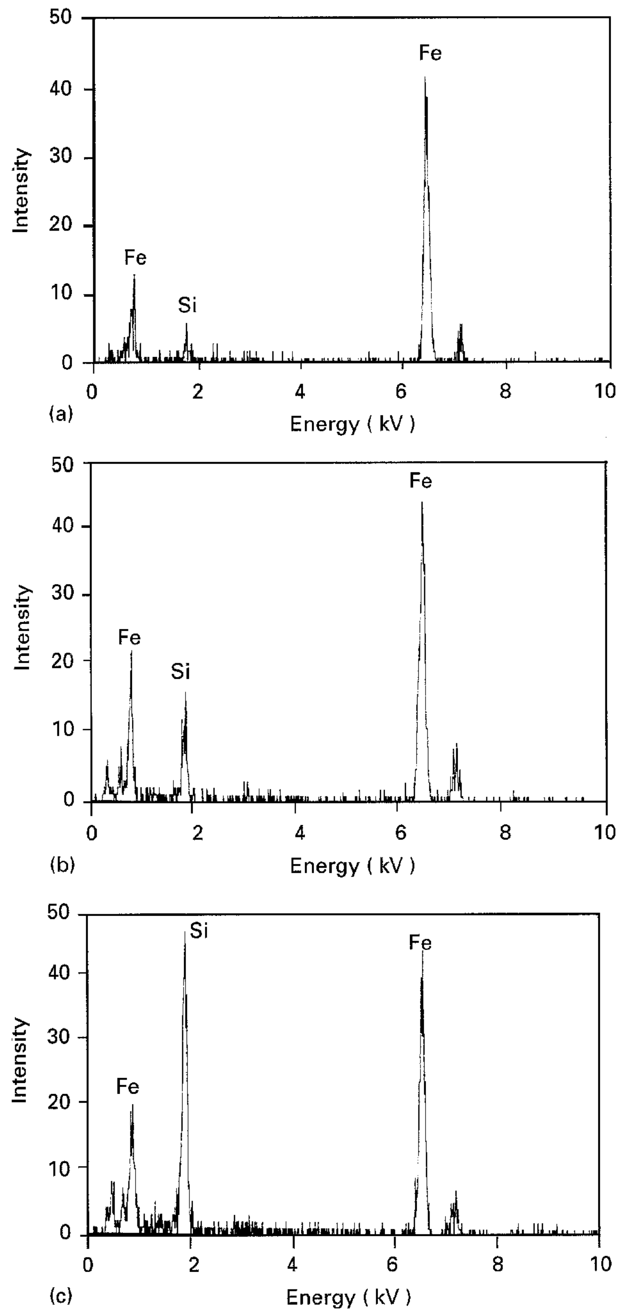

Figure 5 Energy dispersive X-ray (EDX) spectra taken from sample annealed at 400 °C for 2 h: (a) α-Fe grain, (b) Fe_3Si grain, and (c) FeSi layer.

results seem to be contradictory to the findings of Lau *et al.* [17], where Fe_3Si was reported to form from α-Fe through a disorder–order transformation. However, their XRD results were inconclusive, as the reflections attributed to Fe_3Si could have been due to α-Fe, i.e. the (4 2 2) and (4 4 0) reflections for α_1-Fe_3Si have about the same *d* spacings as (2 1 1) and (2 2 0), respectively, for α-Fe. Recent work by the authors on the bulk Fe–Si diffusion couples seems to confirm the above, as thick layers (several tens of micrometres) of Fe_3Si were found to be stoichiometric and microstructurally separate from α-Fe [36].

That FeSi forms initially seems logical from a kinetic standpoint, given that Si is the major diffusing species in low temperature reactions. Once the solubility limit for Si is reached in α-Fe, FeSi, being more Si-rich than Fe_3Si, would form. β-$FeSi_2$ does not form,

TABLE II Indexed SAD results for 400 °C samples

d (nm)	Intensity	Si d (nm)	Si hkl	α-Fe d (nm)	α-Fe hkl	α_1-Fe_3Si d (nm)	α_1-Fe_3Si hkl	FeSi d (nm)	FeSi hkl
30 min at 400 °C									
0.3185	Weak, prefer							0.3174	(1 1 0)
0.2548	Weak							0.2591	(1 1 1)
0.2239	Weak							0.2243	(2 0 0)
0.2025	Strongest			0.2027	(1 1 0)	0.2000	(2 2 0)	0.2008	(2 1 0)
0.1920	Spots	0.1920	(2 2 0)						
0.1844	Fair, prefer							0.1832	(2 1 1)
0.1485	Weak							0.1496	(2 2 1)
0.1442	Strong			0.1433	(2 0 0)	0.1415	(4 0 0)	0.1419	(3 1 0)
0.1332	Weak							0.1353	(3 1 1)
0.1208	Weak							0.1199	(3 2 1)
0.1174	Strong			0.1170	(2 1 1)	0.1156	(4 2 2)		
2 h at 400 °C									
0.3190	Medium, prefer							0.3174	(1 1 0)
0.2834	Medium					0.2830	(2 0 0)		
0.2590	Medium, prefer							0.2591	(1 1 1)
0.2249	Medium, prefer							0.2243	(2 0 0)
0.2004	Strongest			0.2027	(1 1 0)	0.2000	(2 2 0)	0.2008	(2 1 0)
0.1922	Points	0.1920	(2 2 0)						
0.1837	Strong, prefer							0.1832	(2 1 1)
0.1707	Weak					0.1706	(3 1 1)		
0.1640	Weak					0.1632	(2 2 2)		
0.1603	Weak							0.1587	(2 2 0)
0.1508	Weak							0.1496	(2 2 1)
0.1438	Weak							0.1419	(3 1 0)
0.1417	Strong			0.1433	(2 0 0)	0.1415	(4 0 0)		

as discussed below because of its large nucleation barrier. As the FeSi layer thickness increases, the Si flux would decrease, eventually reaching a critical value, where the formation of Fe_3Si becomes kinetically favourable.

At 500 °C, the early stages of the silicide growth sequence progress much faster. A sample, shown in Fig. 6a, annealed for only 15 min, contained a single layer of FeSi ($\approx$75 nm thick) with no Fe_3Si. The silicide layer was the thickness expected for FeSi by mass balance considerations. Samples annealed for 30 min, 1, 1.5, 1.75 and 2 h all looked much like the 15 min sample; a continuous layer of FeSi. No evidence for β-$FeSi_2$ formation could be found in plan views and diffraction analysis indicated no phase other than FeSi. The reason for this contrast in formation times, very short for FeSi and long for β-$FeSi_2$, is explained by the differences in formation kinetics. FeSi grows as a diffusion controlled layer, whereas the formation of β-$FeSi_2$ is considered to be nucleation controlled [7, 31, 32]. Subcritical β-$FeSi_2$ nuclei have been found at 500 °C, however, at annealing times as short as 1 h (Fig. 6b). The tiny β-$FeSi_2$ protrusions between the FeSi and Si were found by searching for grain-to-grain contrast effects while slowly tilting the TEM specimen stage. The β-$FeSi_2$ grains are smaller than almost all the FeSi grains and occur at the FeSi–Si interface with their longest dimension aligned along the interface, presumably to take advantage of the interfacial surface energy available. By comparison, individual FeSi grains usually extend through the entire thickness of the film. EDX analysis confirmed

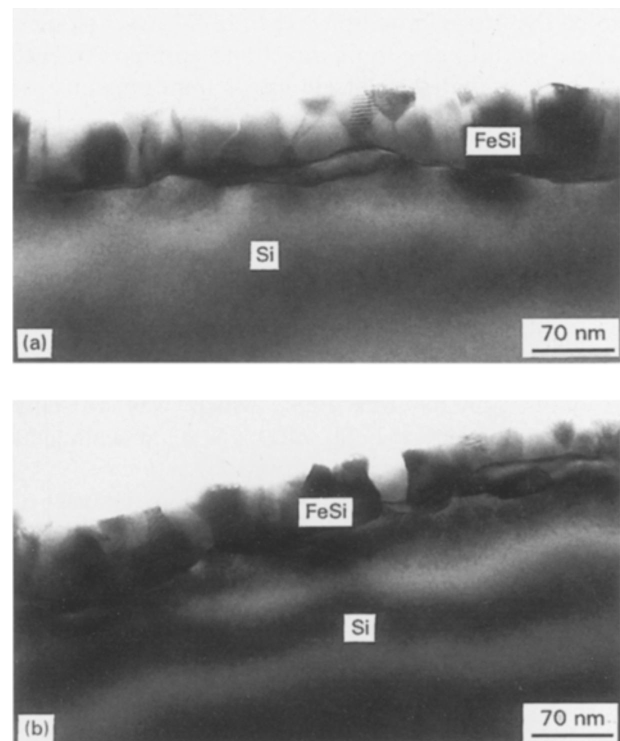

Figure 6 Cross-section image of a sample annealed for (a) 15 min at 500 °C, and (b) 10 min at 500 °C. A subcritical β-$FeSi_2$ nucleus is indicated by the arrow.

that the protrusions were significantly higher in Si content than the main FeSi layer.

Annealing at 600 °C, as at 500 °C, produced completed FeSi layers within 15 min. Unlike the lower

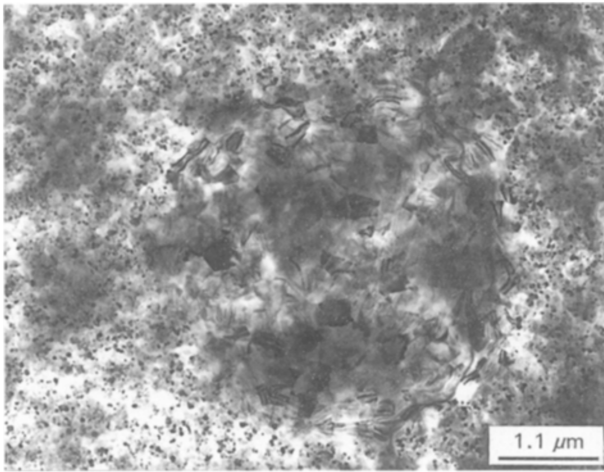

Figure 7 Plan view image of sample annealed at 600 °C for 1 h. A β-$FeSi_2$ colony is visible in the FeSi matrix. Note the difference in grain size between FeSi and β-$FeSi_2$.

temperature anneals, however, the 600 °C samples produced the first growing β-$FeSi_2$ colonies after only about 1 h of heating. Fig. 7 shows one of these colonies in a plan view section. β-$FeSi_2$ covers a circular area and is easily identified by its grain size, which is much larger than that of FeSi. There were only about a dozen colonies like one pictured on the entire sample. The distances separating them were typically at least ten times the width of the colonies.

Although it is generally thought that β-$FeSi_2$ grows by nucleation controlled kinetics, these are believed to be the first micrographs taken of β-$FeSi_2$ colonies. These pictures give more direct and graphic evidence of the way that this silicide grows than previous experimental support has offered.

The β-$FeSi_2$ colonies which form at 600 °C grow radially outward through the silicide film until they contact one another. After 2 h, a small fraction of the film is still FeSi. Only a few tens of grains of FeSi were found in an entire plan view sample after 2.5 h of annealing.

Small β-$FeSi_2$ colonies are found in plan view samples annealed for as little as 7 min at 650 °C. The initial reaction product was FeSi, which was virtually all consumed by β-$FeSi_2$ after 1 h of annealing at 650 °C.

Fig. 8a, b shows high magnification images of the FeSi and β-$FeSi_2$ grain structures, respectively, formed in 650 °C samples, illustrating quite clearly the difference in grain size and morphology between the two phases. FeSi reaches a maximum grain size of ≈40 nm compared with ≈220 nm for β-$FeSi_2$. FeSi grains are much more equiaxed and uniform in size relative to β-$FeSi_2$. Note, also, the profusion of Moiré fringes in the FeSi grains, a result of slight mismatches between the crystallographic spacings–orientations of the overlapping FeSi grains and the Si substrate. Many of the β-$FeSi_2$ grains in Fig. 8b possess internal structure, which has been documented recently by Zheng *et al.* [37] as twinlike structures running along [1 0 0] directions in β-$FeSi_2$. These lamellae were reported to be 0.5–3.0 nm in thickness and highly strained.

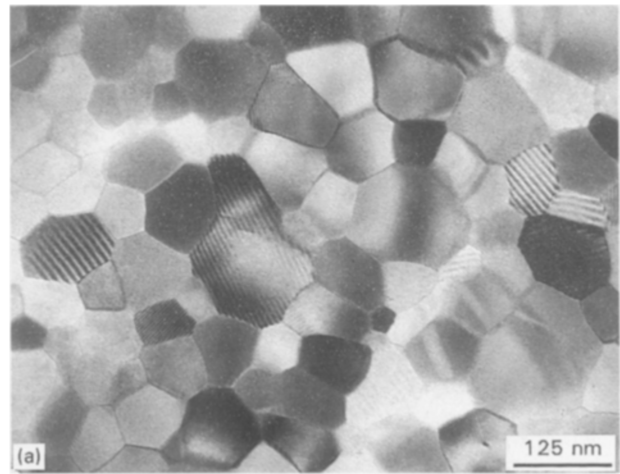

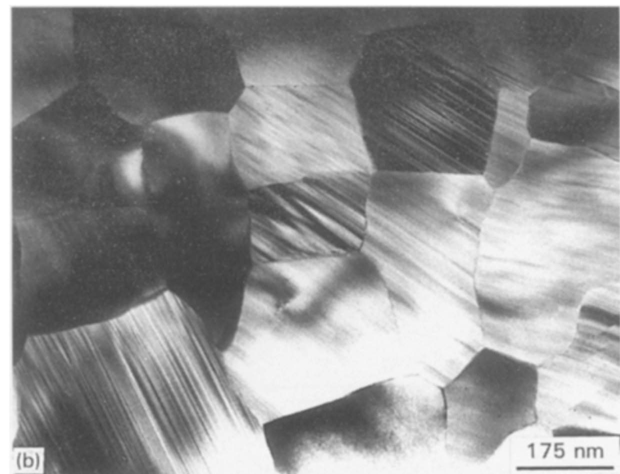

Figure 8 Plan view micrograph, showing (a) FeSi microstructure, of sample annealed at 650 °C for 10 min, and (b) β-$FeSi_2$ sample annealed at 650 °C for 1 h.

4. Conclusions

Two major conclusions can be drawn from the presented work.

1. First of all, it is clear the FeSi forms initially during the annealing of Fe–Si thin film couples. Fe_3Si does form, but not until almost all the α-Fe is consumed, and forms as a distinct phase separate from α-Fe and not through a disorder–order transformation.

2. Clear microstructural evidence was presented that β-$FeSi_2$ forms through a nucleation controlled process.

Acknowledgements

This work was supported by grants from the Natural Sciences and Engineering Research Council (NSERC) of Canada and the Alberta Microelectronic Centre (AMC).

References

1. M. C. BOST and J. E. MAHAN, *J. Appl. Phys.* **58** (1985) 2696.
2. *Idem, ibid.* **64** (1988) 2034.
3. A. RIZZI, H. MORITZ and H. LÜTH, *SPIE* **1361** (1990) 827.
4. *Idem, J. Vac. Sci. Technol. A* **9** (1991) 912.

5. K. LEFKI, P. MURET, N. CHERIEF and R. C. CINTI, *J. Appl. Phys.* **69** (1991) 352.
6. M. DE CRESCENZI, G. GAGGIOTTI, N. MOTTA, F. PATELLA, A. BALZAROTTI, G. MATTOGNO and J. DERRIEN, *Surf. Sci.* **251/252** (1991) 175.
7. C. A. DIMITRIADIS and J. H. WERNER, *J. Appl. Phys.* **68** (1990) 93.
8. N. E. CHRISTENSEN, *Phys. Rev. B* **42** (1990) 7148.
9. W. RAUNAU, H. NIEHUS, T. SCHILLING and G. COMSA, *Surf. Sci.* **286** (1993) 203.
10. W. RAUNAU, H. NIEHUS and G. COMSA, *Surf. Sci. Lett.* **284** (1993) L375.
11. M. POWALLA and K. HERZ, *Appl. Surf. Sci.* **70/71** (1993) 593.
12. C. STUHLMANN, J. SCHMIDT and H. IBACH, *J. Appl. Phys.* **72** (1992) 5905.
13. K. RADERMACHER, O. SKEIDE, R. CARIUS, J. KLOMFAB and S. MANTL, *Mater. Res. Soc. Symp. Proc.* **320** (1994) 115.
14. B. RÖSEN, D. FREUNDT, C. DIEKER, D. GERTHSEN, A. RIZZI, R. CARIUS and H. LÜTH, *ibid.* **320** (1994) 139.
15. H. C. CHENG, L. J. CHEN and T. R. YOUR, *ibid.* **25** (1984) 441.
16. H. C. CHENG, T. R. YEW and L. J. CHEN, *J. Appl. Phys.* **57** (1985) 5246.
17. S. S. LAU, J. S.-Y. FENG, J. O. OLOWOLAFE and M.-A. NICOLET, *Thin Solid Films* **25** (1975) 415.
18. O. KUBASCHEWSKI, "Iron-Binary Phase Diagrams" (Springer-Verlag, New York, 1982) p. 136.
19. J. M. GALLEGO and R. MIRANDA, *J. Appl. Phys.* **69** (1991) 1377.
20. J. ALVAREZ, J. J. HINAREJOS, E. G. MICHEL, J. M. GALLEGO, A. L. VAZQUEZ DE PARGA, J. DE LA FIGUERA, C. OCAL and R. MIRANDA, *Appl. Phys. Lett.* **59** (1991) 99.
21. Q.-G. ZHU, H. IWASAKI, E. D. WILLIAMS and R. L. PARK, *J. Appl. Phys.* **60** (1986) 2629.
22. S. DEGROOTE, M. H. LANGELAAR, T. KOBAYASHI, J. DEKOSTER, J. DE WACHTER, R. MOONS, L. NIESEN and G. LANGOUCHE, *Mater. Res. Soc. Symp. Proc.* **320** (1994) 133.
23. H. von KÄNEL, K. A. MÄDER, E. MÜLLER, N. ONDA and H. SIRRINGHAUS, *Phys. Rev. B* **45** (1992) 13807.
24. N. ONDA, J. HENZ, E. MÜLLER, H. von KÄNEL, C. SCHWARZ and R. E. PIXLEY, *Helv. Phys. Acta* **64** (1991) 197.
25. J. CHEVRIER, V. LE THANH, S. NITSCHE and J. DERRIEN, *Appl. Surf. Sci.* **56–58** (1992) 438.
26. J. ALVAREZ, J. J. HINAREJOS, E. G. MICHEL and R. MIRANDA, *Surf. Sci* **287/288** (1993) 490.
27. U. KAFADER, C. PIRRI, P. WETZEL and G. GEWINNER, *Appl. Surf. Sci.* **64** (1993) 297.
28. M. G. GRIMALDI, P. BAERI, C. SPINELLA and S. LAGOMARSINO, *Appl. Phys. Lett.* **60** (1992) 1132.
29. N. ONDA, J. HENZ, E. MÜLLER, K. A. MÄDER and H. von KÄNEL, *Appl. Surf. Sci.* **56–58** (1992) 421.
30. X. W. LIN, J. DESIMONI, H. BERNAS, Z. LILIENTAL-WEBER and J. WASHBURN, *Mater. Res. Soc. Symp. Proc.* **311** (1993) 293.
31. K. RADERMACHER, S. MANTL, C. DIEKER, H. LÜTH and C. FREIBURG, *Thin Solid Films* **215** (1992) 76.
32. U. ERLESAND, M. ÖSTLING and K. BODÉN, *Appl. Surf. Sci.* **53** (1991) 153.
33. H. von KÄNEL, N. ONDA, H. SIRRINGHAUS, E. MÜLLER-GUBLER, S. GONCALVES-CONTO and C. SCHWARZ, *ibid.* **70/71** (1993) 559.
34. O. P. KARPENKO, C. H. OLK, G. L. DOLL, J. F. MANSFIELD and S. M. YALISOVE, *Mater. Res. Soc. Symp. Proc.* **320** (1994) 103.
35. X. WALLART, J. P. NYS, O. DEHAESE and G. VINCENT, *Appl. Surf. Sci.* **70/71** (1993) 598.
36. N. R. BALDWIN and D. G. IVEY, *J. Phase Equilibria*, submitted.
37. Y. ZHENG, A. TACCOEN, M. GANDAIS and J. F. PÉTROFF, *J. Appl. Cryst.* **26** (1993) 388.

Received 28 April
and accepted 24 May 1995